Computers and Geotechnics 72 (2016) 57–66

Contents lists available at ScienceDirect

Computers and Geotechnics

journal homepage: www.elsevier.com/locate/compgeo

Research Paper

Numerical analysis of penetrometers free-falling into soil with shear strength increasing linearly with depth

M.H. Moavenian [a,b], M. Nazem [a,b,*], J.P. Carter [a,b], M.F. Randolph [a,c]

[a] Australian Research Council Centre of Excellence for Geotechnical Science and Engineering, Australia[1]
[b] The University of Newcastle, Newcastle, NSW, Australia
[c] The University of Western Australia, Australia

ARTICLE INFO

Article history:
Received 23 May 2015
Received in revised form 8 September 2015
Accepted 1 November 2015

Keywords:
Free-falling penetrometer
Dynamic penetration
Site investigation

ABSTRACT

Dynamic penetrometers have been used for offshore oil and gas industry applications such as pipeline feasibility studies and anchoring systems, and military applications including naval mine countermeasures and terminal ballistic studies. The main challenge of using dynamic penetrometers is the interpretation of their test results in order to deduce the mechanical properties of the penetrated soil via empirical or theoretical relations. Recently, a robust numerical method based on the Arbitrary Lagrangian–Eulerian (ALE) technique has been developed for analysing dynamic penetration problems and used to investigate a smooth penetrometer free falling into a uniform layer of clayey soil. Numerical as well as experimental results indicate that the penetration characteristics, including the impact energy, total time, and total depth of penetration, depend on the mechanical properties of the soil including its stiffness and strength parameters as well as the geometry of the penetrometer and its initial impact energy. In this study, the ALE method is employed to study the effect of shear strength increasing with depth (a common condition of seabed deposits) on the penetration characteristics of a free falling penetrometer. Conducting more than two thousand numerical simulations has shown that there is an approximate quadratic relation between the final embedment depth of a FFP penetrating into a non-uniform clay soil and the combined kinetic energy on contact with the soil and subsequent loss in potential energy of the penetrometer.

1. Introduction

In engineering practice, laboratory and in situ tests are used to measure the geotechnical properties of the ground, which are essential in the design and construction of a wide range of physical infrastructure, such as bridges, dams, roads, landfills, pipelines, and offshore platforms. Penetrometers are probably the most popular devices for in situ testing. For instance, the static cone penetration test (CPT) is now a standard in situ testing procedure to explore the geotechnical properties of soil layers as well as their stratigraphy. This test is often conducted for major infrastructure projects in order to gain vital information on soil properties, but it cannot be undertaken easily in sites where the soil is relatively inaccessible such as many deep seabed deposits. On such sites free falling penetrometers (FFP) have been employed to provide information on the mechanical properties of the soil [26].

FFP tests can provide useful data, such as the total depth and time of penetration and the deceleration characteristics of the falling penetrometer. Potentially, these data can then be used to deduce strength parameters for the soil in situ [5,22]. An expendable dynamic penetrometer was used by Beard [3] to measure seafloor penetrability and its undrained shear strength in deep sea regions. A range of dynamic penetrometers were tested by Denness et al. [10] in an attempt to improve data quality and to explore ways of reducing the cost of testing. They recognised that penetrometers can be used not only as an investigation tool, but also as a potential delivery vehicle for radio-active waste canisters. Stoll et al. [31] and Aubeny and Shi [2] used free falling penetrometers to determine the undrained shear strength of seafloor sediments. Stark et al. [29] used the Nimrod free-falling penetrometer to investigate the shear strength of quartz sand as well as carbonate sand in the North Sea. Further investigations on the soil properties obtained from dynamic penetration were conducted by Steiner et al. [30]. Three different types of seabed penetrometer were described and compared by Stoll et al. [32].

* Corresponding author at: Australian Research Council Centre of Excellence for Geotechnical Science and Engineering, Australia.
E-mail address: majidreza.nazem@newcastle.edu.au (M. Nazem).
[1] http://www.cgse.edu.au.

http://dx.doi.org/10.1016/j.compgeo.2015.11.002
0266-352X/

Recent advances in computational methods have facilitated numerical analysis of the cone penetration test. The finite element method is perhaps the most popular approach for analysing penetration problems in geomechanics [1,5,13,15,27,34,36]. The analysis of dynamic penetration is probably one of the most challenging problems in computational geomechanics. From the point of view of geometrical non-linearity, the penetration of objects into layers of soil potentially involves severe mesh distortion and entanglement of elements caused by the large deformations. This usually motivates the application of adaptive finite-element techniques, such as the Arbitrary Lagrangian–Eulerian (ALE) method, which can successfully overcome the mesh distortion issue. Moreover, the analyst must also consider the relative incompressibility of soil during the short period of penetration, the likelihood of material inhomogeneity, nonlinear stress–strain relations, and the rate-dependency of the material being penetrated. High speed impact with the soil and inertia effects during penetration may also be important. The analyst must also be aware of the possible reflection of stress waves in a finite-element domain usually surrounded by fictitious rigid boundaries. More importantly, the boundary conditions of the problem do not remain constant during the analysis, since the interface between the penetrometer and the soil changes continuously during penetration.

Among the important parameters mentioned above, this study considers specifically the effect of inhomogeneity of the soil (in respect of strength varying continuously with depth, rather than interbedded layers of differing properties) on the penetration characteristic of a free-falling penetrometer. It is well known that the shear strength of many soils, including those located on the seabed, usually increases with depth [28], and this variation is often assumed to be linear, at least as a first engineering approximation. Raymond [25] considered this effect on the bearing capacity of large footings as well as embankments. Davis and Booker [8] studied the effect of a linear increase of shear strength with depth on the bearing capacity of clay soils under strip footings by means of the theory of plasticity. They concluded that the surface cohesion (undrained shear strength) and rate of increase of cohesion with depth play important and independent roles in determining the bearing capacity. Merifield et al. [18] studied the pullout capacity of anchors in an undrained layer of clay in which the shear strength increases with depth. Lu et al. [14] conducted a numerical investigation of the effect of non-uniformity of marine clays on the capacity factors of the T-bar, ball and plate penetrometers. It is notable that in all the studies mentioned above it was assumed that penetration of the soil occurred under static conditions, neglecting the effect of inertia forces.

A preliminary study by Nazem and Carter [21] indicated that, in the case of a FFP, the non-uniformity of soil affects its dynamic response. However, until now this effect has not been studied extensively and reported in the literature. This paper describes a comprehensive parametric study conducted to further understand the effect of increasing shear strength with depth on the penetration characteristics of a FFP. This study was achieved by employing a validated numerical approach based on the ALE method previously developed by Nazem et al. [23,22]. Based on the numerical results obtained in the study, relations are established between the total depth of penetration and controlling parameters such as the initial impact energy of the penetrometer and the mechanical properties of the soil including its stiffness, strength (including the gradient with depth) and rate-dependency.

2. Problem definition and assumptions

A free falling penetrometer with a conical tip is allowed to penetrate into a layer of soil in which the undrained shear strength increases linearly with depth. The initial impact velocity, the mass, and the diameter of the penetrometer are assumed to be v_0, m and d, respectively, as shown in Fig. 1. The total depth and the total time of penetration are attained when the FFP comes to rest, and are denoted by p and t_p, respectively. In order to study the effect of the shear strength of soil on the penetration resistance, the initial stress field due to soil weight is ignored, i.e., it is assumed that the initial total stress components are all zero. Due to the relatively rapid penetration, the soil response is considered to be undrained and the soil is modelled as a Tresca material with an associated plastic flow rule. Poisson's ratio of the soil is assumed to be 0.49 to approximate elastic incompressibility. It is assumed that the undrained shear strength of the soil increases with the strain rate according to [12]:

$$s_u = s_{u,ref}\left[1 + \lambda log\left(Max\left(\frac{\dot{\gamma}}{\dot{\gamma}_{ref}}, 1\right)\right)\right] \quad (1)$$

where s_u is the undrained shear strength of soil, $s_{u,ref}$ denotes the reference undrained shear strength measured at a reference strain rate of $\dot{\gamma}_{ref}$, λ is the rate of increase of strength per log cycle of time, and $\dot{\gamma}$ represents the shear strain rate. The value of $\dot{\gamma}_{ref}$ is assumed to be 1%/h (2.78 s^{-1}) [11]. Because of the need to restrict the range of strain rate for which this relationship holds, $s_{u,ref}$ is also a minimum shear strength, ignoring lower strengths that might be measured at even lower strain rates. The effect of ignoring such low strengths is considered negligible for the problem investigated. Eq. (1) is just one of a number of possible equations that could be used to quantify the effect of strain rate on strength (e.g., as discussed by [4]). It has been selected because of its widespread use for clays and its demonstrated applicability to soft, normally or lightly overconsolidated marine soils [16].

As depicted in Fig. 1, it is also assumed that the shear strength of the clay increases linearly with depth according to

$$s_{u,ref(z)} = s_{u,ref(0)} + k_s z \quad (2)$$

where $s_{u,ref(z)}$ and $s_{u,ref(0)}$ are respectively the undrained shear strength at depth z and the ground surface, and k_s represents the

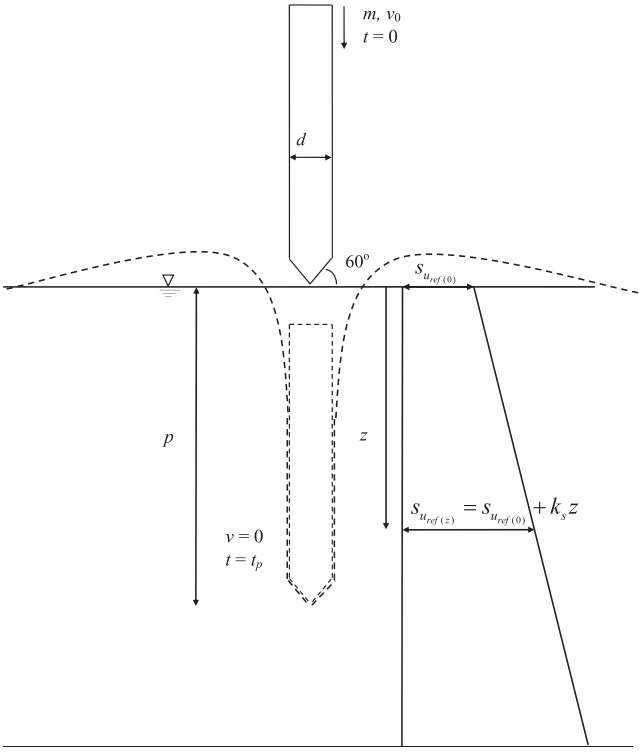

Fig. 1. FTP problem definition.

rate of shear strength increase with depth. To avoid further complexities, the friction between penetrometer and soil and any material damping are ignored in the analyses.

The axisymmetric finite element mesh and the boundary conditions of the problem are shown in Fig. 2. The mesh includes 10,252 nodes and 4,988 6-noded triangular elements. To avoid possible wave reflection, the outer boundary and the bottom of the domain are modelled by the standard viscous (energy absorbing) boundaries introduced by Lysmer and Kuhlemeyer [17]. These boundaries are very efficient in absorbing dilatational waves as well as shear waves in geomechanics problems [17]. The free falling penetrometer is assumed to be rigid.

3. Arbitrary Lagrangian–Eulerian method

The problems of soil penetration involve large deformations, often causing severe mesh distortion and entanglement of elements. Mesh distortion often results in a negative Jacobian of an element, leading to spontaneous termination of the analysis. In some cases of mesh distortion the analysis may not necessarily end, but the highly distorted finite element mesh will potentially produce inaccurate results. To avoid mesh distortion, the ALE method proposed by Nazem et al. [23], and later improved by Nazem et al. [20,22] is employed in this study. This method is based on the operator split technique in which the analysis in each increment is conducted according to the following steps:

- An Updated-Lagrangian (UL) analysis to achieve equilibrium;
- Mesh refinement to eliminate (or to avoid future) mesh distortion; and
- An Eulerian step to remap all state variables from the old mesh to the new mesh.

These steps are briefly explained as follows.

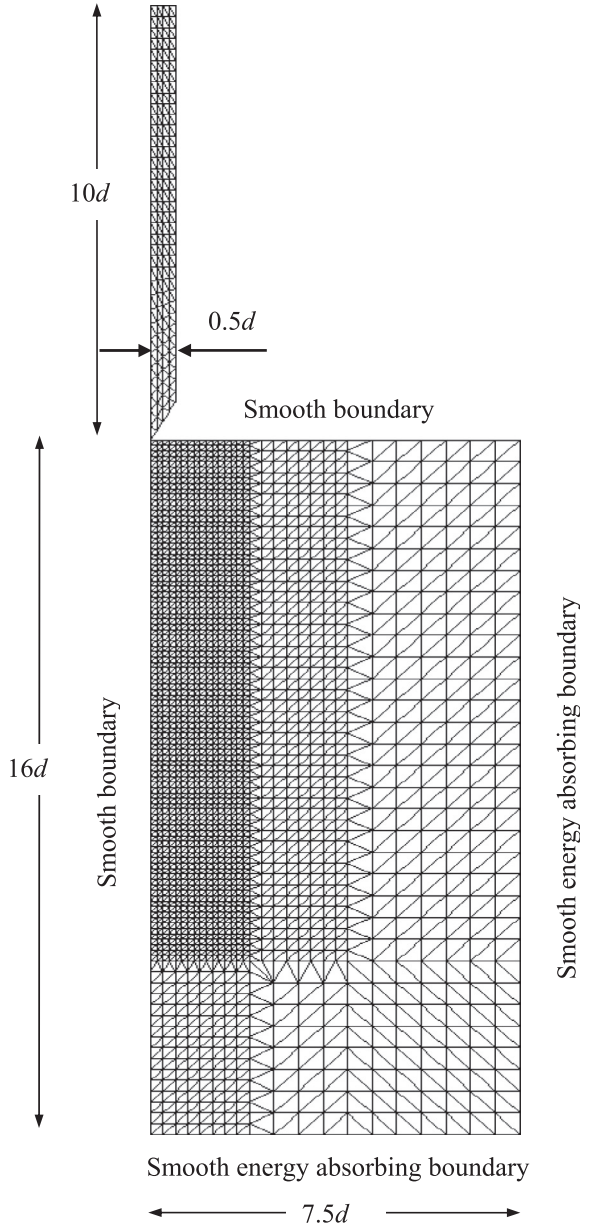

Fig. 2. Finite element mesh and boundary conditions of FFP problem.

3.1. The Updated Lagrangian method

In the UL method, the analysis starts at time 0 and it is assumed that all state variables satisfying equilibrium at time t are known. Dynamic equilibrium will be achieved at time $t+\Delta t$ provided the equation of motion is satisfied, i.e.,

$$\mathbf{M}\ddot{\mathbf{u}}^{t+\Delta t}+\mathbf{C}\dot{\mathbf{u}}^{t+\Delta t}+\mathbf{F}_{int}^{t+\Delta t}=\mathbf{F}_{ext}^{t+\Delta t} \tag{3}$$

where $\mathbf{M}$ and $\mathbf{C}$ are the mass and damping matrices, respectively, $\mathbf{u}$ represents the displacement vector, $\mathbf{F}_{int}$ and $\mathbf{F}_{ext}$ are the internal and the external force vectors, respectively. To solve the momentum equation in (3), the implicit generalised-α method developed by Chung and Hulbert [7] has been employed. Nazem et al. [22] showed the efficiency of this method in solving dynamic penetration problems of soil mechanics. In the generalised-α method, the displacements and velocities are computed using Newmark's method, i.e.,

$$\begin{aligned}\ddot{\mathbf{u}}^{t+\Delta t}&=\tfrac{1}{\beta\Delta t^2}(\mathbf{u}^{t+\Delta t}-\mathbf{u}^{t})-\tfrac{1}{\beta\Delta t}\dot{\mathbf{u}}^{t}-\tfrac{1-2\beta}{2\beta}\ddot{\mathbf{u}}^{t}\\ \dot{\mathbf{u}}^{t+\Delta t}&=\tfrac{\alpha}{\beta\Delta t}(\mathbf{u}^{t+\Delta t}-\mathbf{u}^{t})+\left(1-\tfrac{\alpha}{\beta}\right)\dot{\mathbf{u}}^{t}+\left(1-\tfrac{\alpha}{2\beta}\right)\ddot{\mathbf{u}}^{t}\end{aligned} \tag{4}$$

where α and β are the Newmark integration parameters and Δt represents the time step. Two additional integration parameters, α_f and α_m, are introduced into the momentum equation to compute the inertia forces at time $t+(1-\alpha_m)\Delta t$ and the internal and damping forces at time $t+(1-\alpha_f)\Delta t$. The momentum equation may then be written as follows:

$$\begin{aligned}&\mathbf{M}[(1-\alpha_m)\cdot\ddot{\mathbf{u}}^{t+\Delta t}+\alpha_m\cdot\ddot{\mathbf{u}}^{t}]+\mathbf{C}[(1-\alpha_f)\cdot\dot{\mathbf{u}}^{t+\Delta t}+\alpha_f\cdot\dot{\mathbf{u}}^{t}]\\ &\quad+(1-\alpha_f)\mathbf{F}_{int}^{t+\Delta t}+\alpha_f\cdot\mathbf{F}_{int}^{t}=(1-\alpha_f)\cdot\mathbf{F}_{ext}^{t+\Delta t}+\alpha_f\cdot\mathbf{F}_{ext}^{t}\end{aligned} \tag{5}$$

The differential equation in (5) can be solved by an iterative scheme. Employing the Newton–Raphson method and assuming $\mathbf{K}_T$ represents the tangential stiffness matrix, the following nonlinear equation must be solved in the ith iteration

$$\begin{aligned}&\left[\frac{1-\alpha_m}{\beta\cdot\Delta t^2}\cdot\mathbf{M}+\frac{\alpha(1-\alpha_f)}{\beta\cdot\Delta t}\cdot\mathbf{C}+(1-\alpha_f)\cdot\mathbf{K}_{T(i-1)}\right]\cdot\Delta\mathbf{u}_{(i)}\\ &=(1-\alpha_f)\cdot\mathbf{F}_{ext}^{t+\Delta t}+\alpha_f\cdot\mathbf{F}_{ext}^{t}-(1-\alpha_f)\cdot\mathbf{F}_{int\,(i-1)}^{t+\Delta t}-\alpha_f\cdot\mathbf{K}_{T(i-1)}\cdot\mathbf{u}^{t}\\ &\quad-\mathbf{M}\left[\frac{1-\alpha_m}{\beta\cdot\Delta t^2}\cdot\left(\mathbf{u}_{(i-1)}^{t+\Delta t}-\mathbf{u}^{t}\right)-\frac{1-\alpha_m}{\beta\cdot\Delta t}\cdot\dot{\mathbf{u}}^{t}-\left(\frac{1-\alpha_m}{2\beta}-1\right)\cdot\ddot{\mathbf{u}}^{t}\right]\\ &\quad-\mathbf{C}\left[\frac{\alpha(1-\alpha_f)}{\beta\cdot\Delta t}\cdot\left(\mathbf{u}_{(i-1)}^{t+\Delta t}-\mathbf{u}^{t}\right)+\left(1-\frac{\alpha}{\beta}(1-\alpha_f)\right)\cdot\dot{\mathbf{u}}^{t}\right.\\ &\quad\left.-\Delta t\left(\frac{\alpha}{2\beta}-1\right)(1-\alpha_f)\cdot\ddot{\mathbf{u}}^{t}\right]\mathbf{u}_{(i)}^{t+\Delta t}=\mathbf{u}_{(i-1)}^{t+\Delta t}+\Delta\mathbf{u}_{(i)},\quad\mathbf{u}_{(0)}^{t+\Delta t}=\mathbf{u}^{t}\end{aligned} \tag{6}$$

3.2. Mesh refinement

At the end of the UL step, the nodal coordinates are updated according to the incremental displacements that satisfy equilibrium. In problems with relatively large deformations, such as penetration problems, updating the nodal coordinates may lead to mesh distortion. In the ALE method, mesh refinement is conducted to eliminate possible mesh distortion by changing and optimising the location of the nodal points without modifying the topology of the problem. Since the mesh motion is arbitrary in the ALE method, there are several possibilities to find an optimum mesh. A common method to optimise the mesh involves re-meshing the domain by using a structured mesh generation algorithm that retains a constant topology (including the number of nodes, the number of elements and their connectivity) during the analysis. However, structured mesh generation algorithms are usually applicable to regions with simple geometries. Nazem et al. [23] developed a robust method for mesh optimisation, which makes use of a static elastic analysis. The procedure for mesh optimisation by this method includes two steps: relocation of the nodes along the boundaries and a subsequent elastic analysis. In this context the "boundaries" include the physical boundaries of the problem domain, the material interfaces and the loading boundaries. In the first step, the nodes on the boundaries are relocated along these boundaries (see [19] and [22] for details), providing the spatial locations of the mesh points, $\mathbf{x}_i^r$, for only those nodes along the boundaries. For these nodes, the incremental mesh displacements $\Delta\mathbf{u}_i^r$ are obtained from:

$$\Delta\mathbf{u}_i^r = \mathbf{x}_i^r - \mathbf{x}_i + \Delta\mathbf{u}_i \tag{7}$$

where $\mathbf{x}_i$ represents the spatial locations of material points (obtained at the end of UL step). The known displacements of all nodes on the boundaries, $\Delta\mathbf{u}_i^r$, are then applied to the undeformed domain as prescribed displacements and an elastic analysis using these boundary conditions is performed. This analysis assumes isotropic linear elasticity of a homogeneous medium and small deformation theory and aims to find the incremental displacements for the remaining (interior) nodes of the continuum. The incremental displacement components computed for each node from this elastic analysis are then added to the nodal coordinates of the mesh to find the locations of the nodes in the new mesh. The new mesh and the old mesh share the same connectivity. Such an elastic analysis is very fast and will result in an optimum mesh if the nodes on the boundaries are optimally located.

3.3. Eulerian step

In this step, all state variables at nodal points as well as integration points are mapped from the old mesh to the new mesh. Remapping is usually performed using a first order expansion of Taylor's series, unless higher terms are required. For an arbitrary function f, we can write

$$\dot{f}^r = \dot{f} + (\dot{u}_i^r - \dot{u}_i)\cdot\frac{\partial f}{\partial x_i} \tag{8}$$

where $\dot{f}^r$ and $\dot{f}$ denote the time derivatives of f with respect to the mesh and material coordinates, respectively.

The ALE procedure explained above is summarised in the following algorithm:

1. Assemble the global stiffness matrix and load vector and solve the momentum equation according to (6).
2. Compute the strain increments and integrate the constitutive equations to update the stresses.
3. Repeat Steps (1) and (2) until the unbalanced forces are smaller than a prescribed tolerance.
4. Update the material coordinates according to the incremental displacements.
5. Check the boundaries and relocate the nodes on the boundaries wherever necessary.
6. Compute the new mesh coordinates by performing an elastic analysis.
7. Remap the state variables at integration points as well as at nodal points using Eq. (8).
8. Update the total displacement vector according to the new mesh displacements and previous material displacements.
9. Set the material coordinates equal to the mesh coordinates for the next time step.
10. Compute internal forces, check equilibrium as well as plasticity consistency and conduct further iterations if necessary.

4. Parametric study

4.1. Introduction

Nazem et al. [20] implemented the ALE method explained in the previous section into SNAC, a finite element code developed at the University of Newcastle especially for geotechnical problems. For dynamic penetration problems, SNAC was validated by comparing its predictions with those of other numerical approaches [35]. Predictions have also been shown to agree well with experimental results obtained from FFP tests conducted in the laboratory at the University of Sydney [22]. SNAC is employed here to study the dynamic penetration of a FFP into an inhomogeneous layer of soil in which the undrained shear strength increases linearly with depth.

To study the effect of inhomogeneity of the soil on its dynamic behaviour as well as the penetration characteristics, a total of approximately 2,300 cases were analysed using different values of the problem parameters, as summarised in Table 1. These parameters include:

- d, the diameter of the penetrometer;
- m, the mass of the penetrometer;
- v_0, the impact velocity of the penetrometer;
- $s_{u,ref(0)}$, the undrained shear strength of the soil at the ground surface;
- I_r, the rigidity index of the soil (the ratio between its shear modulus, G, and its undrained shear strength, $s_{u,ref}$);
- λ, the rate parameter for strength defined in Eq. (1); and
- $\bar{k}_s$, a normalised inhomogeneity factor for the soil strength.

A further (constant) parameter that affects the problem is earth's acceleration due to gravity, g.

Typical values of k_s for soft clays are 1–3 kPa/m, although much higher strength gradients are common in the upper 0.5–1 m of penetration in many offshore deposits, where crustal features may occur [9]. The detailed profile in the upper 1 m will affect the penetration characteristics of FFPs, owing to their relatively small

Table 1
Values of parameters used in parametric study.

Variable	Unit	Values
d	m	0.04, 0.06, 0.08, 0.1
m	kg	0.1, 0.5, 1.0, 5.0
v_0	m/s	5.0, 10.0
$s_{u,ref(0)}$	kPa	1.0, 2.0, 4.0
I_r		33, 67, 167
λ		0.0, 0.1, 0.2, 0.3, 0.4, 0.5
$\bar{k}_s$		0.0, 0.05, 0.1, 0.25, 0.5, 0.75, 1.0

diameter, e.g., 40–60 mm for a typical cone penetrometer. However, for simplicity only simple linear strength profiles (Eq. (2)) are considered in this paper. A normalised parameter, $\bar{k}_s$, is adopted in this study which can quantify the significance of the rate of shear strength increase on the penetration, and this parameter is defined by

$$\bar{k}_s = \frac{k_s d}{s_{u,ref(0)}} \tag{9}$$

For each case investigated, the results reported include the total time of penetration, the total depth of penetration, and the dynamic soil resistance. The final penetration depth, p, can be normalised by the penetrometer diameter, d, providing a normalised depth of penetration denoted by $\bar{p}$. To avoid relatively shallow penetration, cases for which $\bar{p} \leqslant 2$ were excluded in this numerical investigation. In addition, due to the limited size of the finite element mesh adopted, cases satisfying $\bar{p} \geqslant 12$ were not considered in this parametric study.

4.2. Impact energy versus geotechnical properties of soil

In a previous study for uniform strength soils, Nazem et al. [22] showed that an appropriate strategy for studying the dynamic penetration problem is to plot the initial impact energy of the penetrometer, i.e., its kinetic energy upon first impact with the soil surface, $0.5\ m v_0^2$, normalised by the quantity $0.25\pi d^3 s_{u,ref(0)}$, versus the normalised depth of penetration, $\bar{p}$. However, the total energy loss during penetration also includes the loss of potential energy due to the penetration of the FFP below the surface of the soil [24]. By including the potential energy, this normalised energy is therefore defined as

$$E_n = \left(\frac{\frac{1}{2}m v_0^2 + mgp}{\frac{1}{4}\pi d^3 s_{u,ref(0)}}\right) = \left(\frac{2m v_0^2 + 4mgp}{\pi d^3 s_{u,ref(0)}}\right) = \left(\frac{2m v_0^2}{\pi d^3 s_{u,ref(0)}}\right) + \left(\frac{4mg\bar{p}}{\pi d^2 s_{u,ref(0)}}\right) \tag{10}$$

For non-uniform strength soils, several functions including linear, logarithmic, exponential and polynomial were examined to find the best relation among the normalised energy, penetration depth and the geotechnical properties of soil. This meticulous examination resulted in a quadratic relation between the normalised kinetic and potential energy, $\bar{E}_n$, given by

$$\bar{E}_n = \frac{E_n}{[0.1 + \ln(I_r)](-4\lambda^2 + 8\lambda + 0.8)} \tag{11}$$

and the normalised penetration $\bar{p}$, in the form of

$$\bar{E}_n = A_s \bar{p}^2 + B_s \bar{p} \tag{12}$$

where A_s and B_s are two variables depending on $\bar{k}_s$. Eqs. (11) and (12) present two formulations with different parameters for $\bar{E}_n$. To study the latter relationship in detail, the normalised energy $\bar{E}_n$ obtained from Eq. (11) is plotted versus the normalised depth of penetration $\bar{p}$ in Fig. 3 for all cases considered (~2300). For each value of $\bar{k}_s$, variables A_s and B_s are obtained and are summarised in Table 2, from which A_s and B_s can be estimated according to

$$\begin{aligned} A_s &\approx 0.052 + 1.353\bar{k}_s \\ B_s &\approx 2.279 - 1.577\bar{k}_s \end{aligned} \tag{13}$$

Substituting the values of A_s and B_s from Eq. (13) in Eq. (12) provides

$$\bar{E}_n = (0.052 + 1.353\bar{k}_s)\bar{p}^2 + (2.279 - 1.577\bar{k}_s)\bar{p} \tag{14}$$

To demonstrate the accuracy of Eq. (14), the normalised energy $\bar{E}_n$ predicted by this equation, and the normalised energy calculated by Eq. (11) are plotted in Fig. 4, according to which there is relatively good agreement between the values predicted by the proposed Eq. (14) and the values of $\bar{E}_n$ used in the analyses. To represent the variation of $\bar{E}_n$ versus $\bar{k}_s$ and $\bar{p}$, Eq. (14) is plotted in three-dimensional space in Fig. 5, which shows that the depth of penetration increases with normalised energy, whereas it decreases with increasing $\bar{k}_s$.

For the special case of a uniform soil layer ($\bar{k}_s = 0$), Eq. (14) is compared with the equations proposed by Nazem et al. [22] in Fig. 6. According to plots in Fig. 6, the values of normalised energy predicted by Eq. (14) are in good agreement with those previously reported for penetrometers falling freely into a uniform layer of soil, although with some divergence due to the use of total energy, rather than kinetic energy at impact, in the current work.

4.3. Soil resistance

In static cone penetration tests, the undrained shear strength of the soil is related to the net cone resistance, q_{net}, by a static cone factor, N_{kt}, according to

$$q_{net} = N_{kt} s_u \tag{15}$$

Numerical and experimental studies suggest that the cone factor depends on the rigidity index of the soil, assuming the soil layer is uniform, the cone is smooth, the penetration rate is slow enough to ignore the inertia effects and, on the other hand, is fast enough to neglect the effect of partial consolidation occurring around the tip of the cone during penetration [13,22,33,34,36]. Among others, some of the expressions derived for the static cone factor from numerical modelling are as follows:

$$N_{kt} = 1.25 + 1.84\ln(I_r) \quad \text{(Teh and Houlsby [33])} \tag{16}$$

$$N_{kt} = 0.33 + 2\ln(I_r) \quad \text{(Yu et al. [36])} \tag{17}$$

$$N_{kt} = 1.0 + 1.825\ln(I_r) \quad \text{(Liyanapathirana [13])} \tag{18}$$

$$N_{kt} = 3.4 + 1.6\ln(I_r) \quad \text{(Lu et al. [14])} \tag{19}$$

$$N_{kt} = 2.32 + 1.69\ln(I_r) \quad \text{(Nazem et al. [22])} \tag{20}$$

Eqs. (16–18) are based on the von Mises soil model, whereas the Tresca soil model has been used in deriving Eqs. (19) and (20).

In the problems considered in this study it is assumed that the undrained shear strength of the soil increases linearly with depth. This suggests that the dynamic soil resistance, q_{dyn}, will not generally approach a constant value representing a steady state (but might do if normalised by the local shear strength), but will increase as the object penetrates into the soil. To show this effect, the soil resistance normalised by its undrained shear strength at the ground surface, $s_{u,ref(0)}$, is plotted versus the normalised penetration $\bar{p}$ in Fig. 7 for the case where $\bar{k}_s = 0.5$, $\lambda = 0.4$, and $I_r = 167$ as well as the case where $\bar{k}_s = 0.25$, $\lambda = 0.2$, and $I_r = 67$. The dynamic soil resistance initially increases rapidly due to the inertial effects caused by the impact of the penetrometer and the soil, and then increases more or less in a linear fashion with penetration after the inertial effects have reduced relative to the geotechnical resistance. This trend is observed for every specimen penetrating into a non-uniform layer of soil, i.e., for $\bar{k}_s \neq 0$. The initially high dynamic resistance on impact is typical of experimental FFP data [6]. An alternative and interesting way to investigate the dynamic soil resistance is to plot the net dynamic pressure acting on the penetrometer, normalised by the undrained shear strength of soil at the current depth of penetration, $s_{u,ref(z)}$, versus $\bar{p}$, as

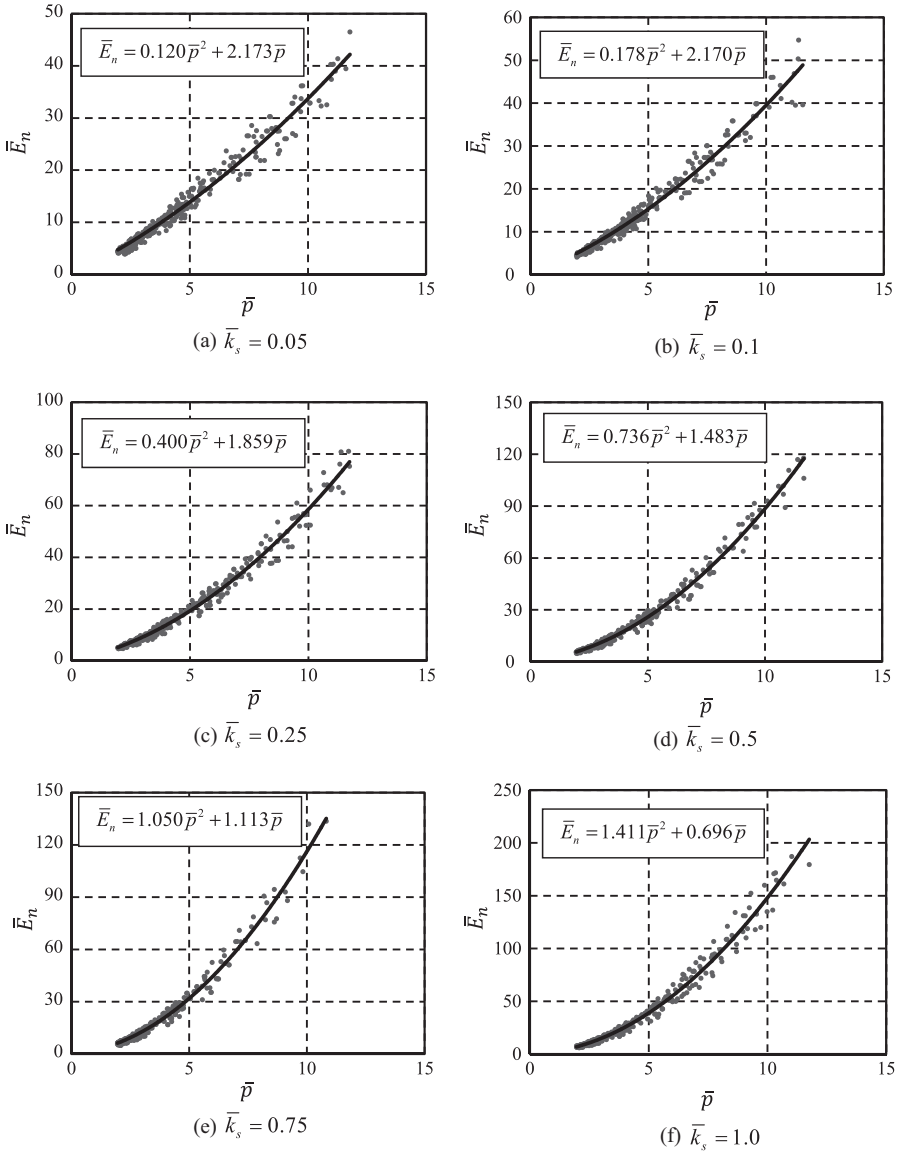

Fig. 3. Normalised energy $\bar{E}_n$ versus normalised penetration $\bar{p}$.

Table 2
Values of A_s and B_s.

$\bar{k}_s$	A_s	B_s
0.05	0.120	2.173
0.1	0.178	2.170
0.25	0.4	1.859
0.5	0.736	1.483
0.75	1.05	1.113
1.0	1.411	0.696

shown in Fig. 8. The normalised soil resistance then approaches a more or less constant value, which depends on I_r and λ, but not necessarily on $\bar{k}_s$. The dynamic cone penetration factor, N_{dp}, can thus be defined as

$$N_{dp} = \frac{q_{dyn(z)}}{s_{u,ref(z)}} = \frac{q_{dyn(z)}}{s_{u,ref(0)} + k_s z} \tag{21}$$

where $q_{dyn(z)}$ represents the net pressure on the penetrometer when it reaches a depth z, which is determined by dividing the vertical component of the resultant force at the interface between the penetrometer and soil by $\pi d^2/4$.

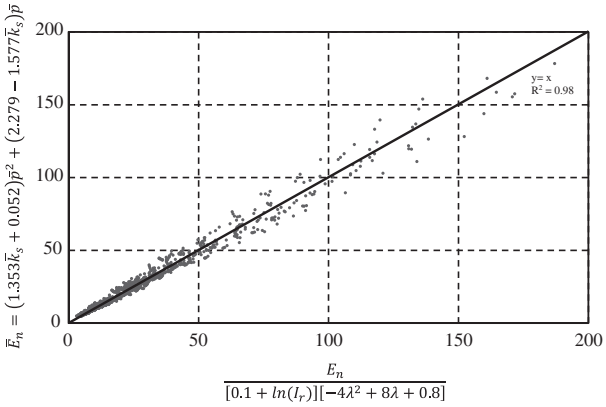

Fig. 4. Comparison of the values of $\bar{E}_n$ estimated by Eq. (14) and the input values of the finite element analyses obtained from Eq. (10).

Note that for $\bar{k}_s = 0$, i.e., a homogeneous soil layer, the soil resistance converges to a constant that depends on the rate parameter λ, the rigidity index I_r, and $\bar{p}$ [22]. According to Nazem et al. [22],

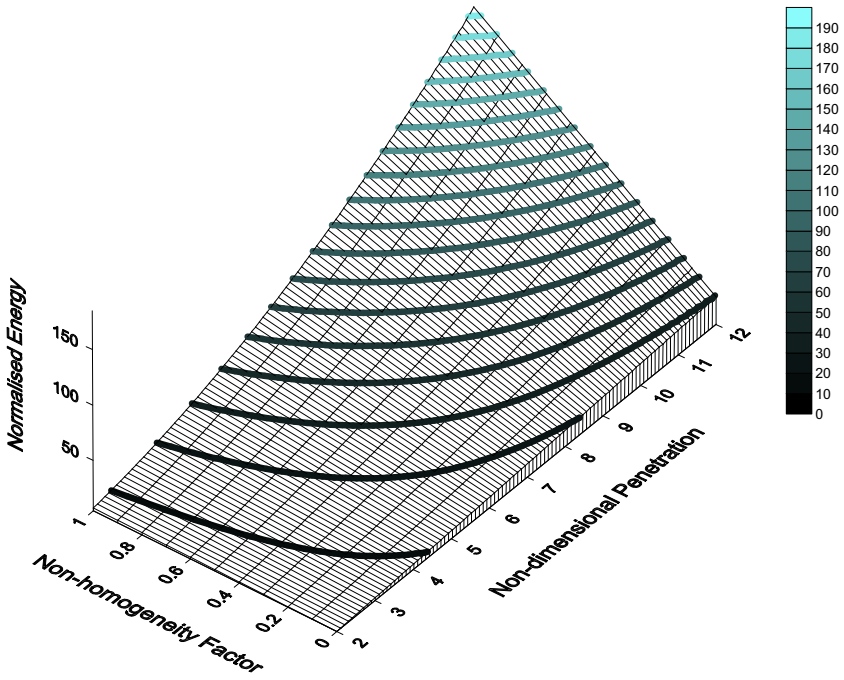

Fig. 5. $\bar{E}_n$ versus $\bar{p}$ and $\bar{k}_s$.

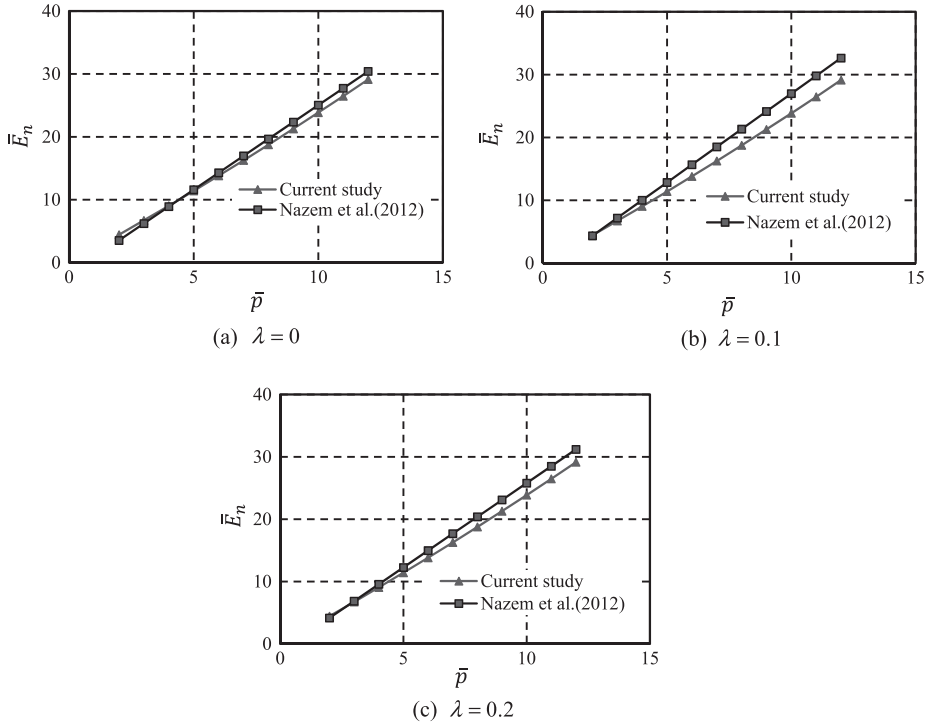

Fig. 6. Comparison of the equation proposed by Nazem et al. [22] with the formula obtained in current study for homogeneous clay soils ($\bar{k}_s = 0$) and $I_r = 33.3$.

this constant value, N_{dp}, which is similar to the cone factor N_{kt} in a static cone penetration test, may be obtained by

$$N_{dp} = 2.321 - 50.488\lambda + (1.69 + 34.546\lambda)\ln(I_r) + \frac{1}{\bar{p}}(2.698 + 148.36\lambda + 410.27\lambda^2 - (2.399 + 46.52\lambda - 103.91\lambda^2)\ln(I_r)) \quad (22)$$

For a relatively large depth of penetration ($\bar{p} \to \infty$), the second term in Eq. (22) can be ignored, providing

$$N_{dp} \simeq 2.321 - 50.488\lambda + (1.69 + 34.546\lambda)\ln(I_r) \quad (23)$$

In order to study the effect of the rate parameter (λ) on the normalised cone resistance, N_{dp} is plotted against rate parameter (λ) for different values of I_r in Fig. 9. Note that values of N_{dp} have been obtained by finding the average values of soil resistance, normalised by the undrained shear strength (at the penetration depth), obtained in the last half diameter of penetration. For a given value of λ, it may be shown that the normalised cone resistance increases linearly with ln I_r. Furthermore, for a constant

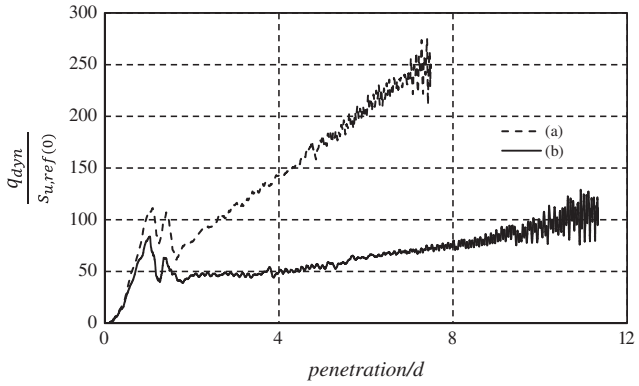

Fig. 7. Dynamic soil resistance normalised by $s_{u,ref(0)}$ versus normalised penetration for (a) $\bar{k}_s = 0.5$, $\lambda = 0.4$, and $I_r = 167$ and (b) $\bar{k}_s = 0.25$, $\lambda = 0.2$, and $I_r = 67$.

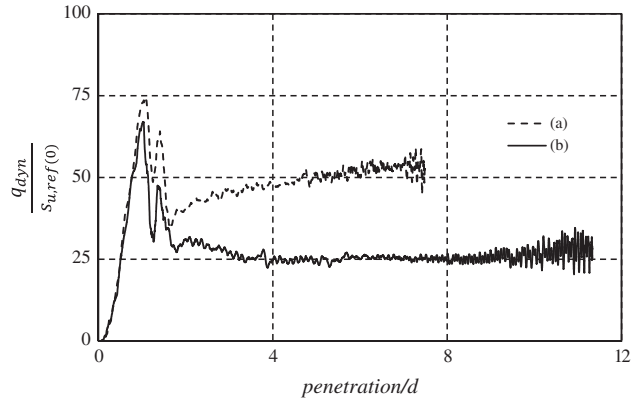

Fig. 8. Dynamic soil resistance normalised by $s_{u,ref(z)}$ versus normalised penetration for (a) $\bar{k}_s = 0.5$, $\lambda = 0.4$, and $I_r = 167$ and (b) $\bar{k}_s = 0.25$, $\lambda = 0.2$, and $I_r = 67$.

value of rigidity index, the soil resistance increases with increasing λ. According to these observations the following equation is obtained by a process of curve-fitting using all numerical results

$$N_{dp} = \frac{q_{dyn,z}}{s_{u,ref(z)}} \simeq (2.89 - 78.96\lambda - 34.21\lambda^2) + (1.64 + 43.84\lambda - 8.93\lambda^2)\ln(I_r) + \frac{1}{\bar{p}}[7.72 + 101.65\lambda - 74.84\lambda^2 + (-4.38 - 30.38\lambda + 26.58\lambda^2)\ln(I_r)] \quad (24)$$

For the special case of a rate independent soil and deep penetration ($\lambda = 0$ and $\bar{p} \to \infty$):

$$N_{dp} = \frac{q_{dyn,z}}{s_{u,ref(z)}} \simeq 2.89 + 1.64\ln(I_r) \quad (25)$$

In the case where $\lambda = 0$, the dynamic cone penetration factors predicted by Eq. (25) are compared with the values predicted by Eqs. (16–19), i.e., those currently available in the literature, in Fig. 10. According to this figure, there is relatively good agreement between the current study and previous work.

4.4. Deceleration and velocity specifications

To study the deceleration characteristics of the penetrometer, its velocity normalised by the initial impact velocity and its acceleration normalised by the gravitational acceleration, g, versus time are plotted in Figs. 11 and 12, respectively, for penetration into both a non-uniform and uniform soil layer. According to Fig. 12, the magnitude of the deceleration of a FFP penetrating into a uniform layer of soil is approximately constant, whereas the magnitude of this deceleration increases linearly with time for a non-uniform layer of soil. Fig. 11 also indicates that the velocity of a FFP reduces approximately linearly or quadratically for penetrations into a uniform and a non-uniform soil layer, respectively. The linearly increasing deceleration as well as the quadratic changes in velocity that occur as the penetrometer becomes embedded in the soil are due to the linear increase in shear strength of the soil with depth. On the other hand the deceleration curve is more or less flat for a uniform soil and the velocity changes almost linearly with time. It can be concluded that the form of deceleration of a penetrometer is highly dependent on the undrained shear strength of a soil and how that strength might vary with depth.

5. Interpretation of FFP tests

The use to which the numerical solutions presented previously may be put in interpreting the results of FFP tests is best illustrated with an example.

Consider the case where a FFP with a conical tip of diameter 0.08 m (80 mm), weighing 52 kg in air is allowed to free fall through the water column penetrating the seabed. The velocity at impact with the seabed is assumed to be 2 m/s. It is noted that these dimensions of the FFP are representative of at least one probe used in practice (e.g., see http://www.brooke-ocean.com/ffcpt-01.html).

Some FFPs are instrumented to measure more than just the final penetration. Indeed, the more sophisticated devices are instrumented to measure accelerations, cone resistance and pore water pressures during the entire penetration of the seabed. However, at present we confine attention to measurements of the ultimate penetration, using that single piece of information to interpret

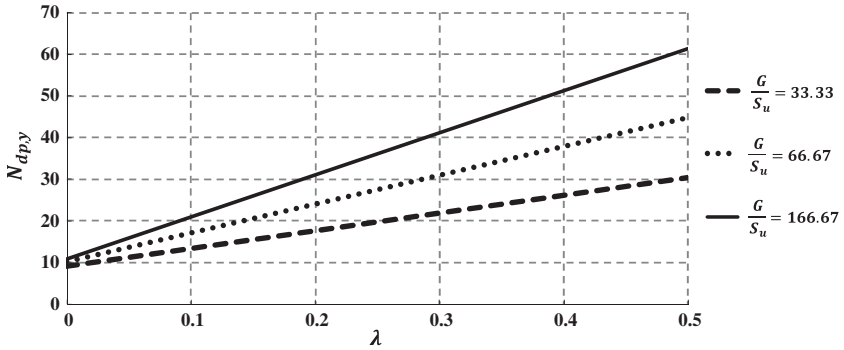

Fig. 9. Normalised cone resistance pressure against λ for $G/s_u = 33.33$, 66.67 and 166.67.

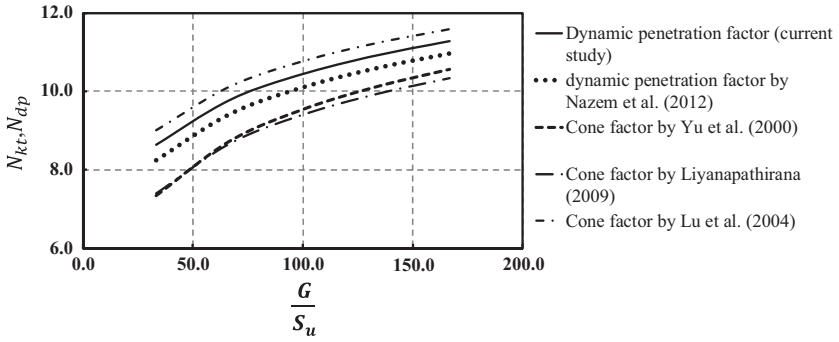

Fig. 10. Static and dynamic cone factors against $\frac{G}{s_{u,ref}}$.

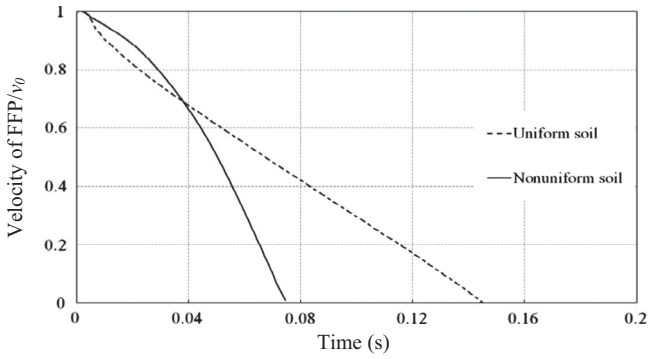

Fig. 11. Velocity profile of a FFP in non-uniform and uniform layers of soil.

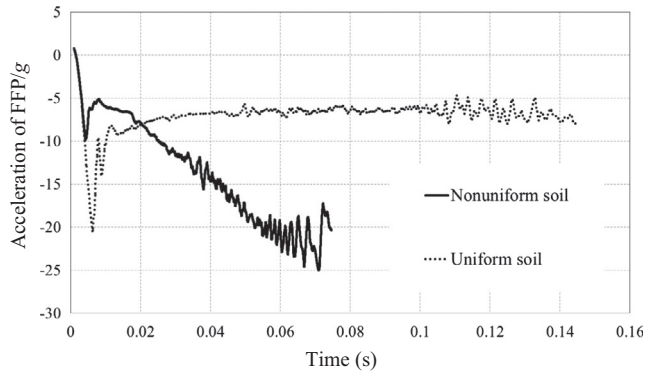

Fig. 12. Acceleration of a FFP in non-uniform and uniform layers of soil.

the soil strength properties. In practice, additional insight into the soil strength profile becomes possible if the deceleration profile is monitored during penetration (e.g., see Fig. 12), but that aspect is not pursued further here.

For a seabed idealised as in the numerical study described previously, i.e., a Tresca material with a rate-dependent undrained shear strength that may vary linearly with depth below mudline, then four parameters are required to define the undrained strength and its profile, viz., $s_{u,ref(0)}$, k_s, λ and I_r. Obviously, a definitive determination of each parameter is not possible from only one field measurement. However, fortunately, typical values and ranges are known for some of these parameters for undrained fine-grained sea bed soils. For example, typically, k_s varies from 0 to 3 kPa/m, λ is typically in the range from 0 (for a rate independent strength) to 0.4, and typically I_r varies from 50 to 100 for medium to high plasticity clays.

If we consider these specific ranges for k_s, λ and I_r, then we may use the other given information about the penetrometer, i.e., its mass, velocity, size and final penetration to interpret typical values of the reference shear strength $s_{u,ref(0)}$. This can be achieved by appropriate application of Eq. (14), and the results for this example case are presented graphically in Fig. 13a for the case where the final penetration is 0.2 m, and in Fig. 13b where the final penetration is assumed to be 1.2 m.

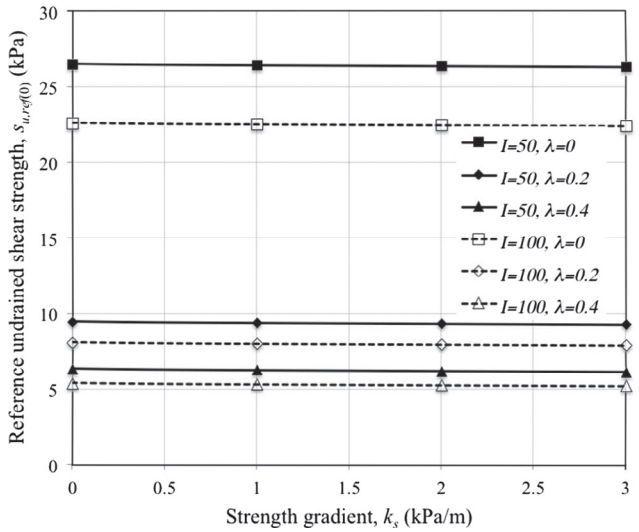

(a) 0.2 m final penetration

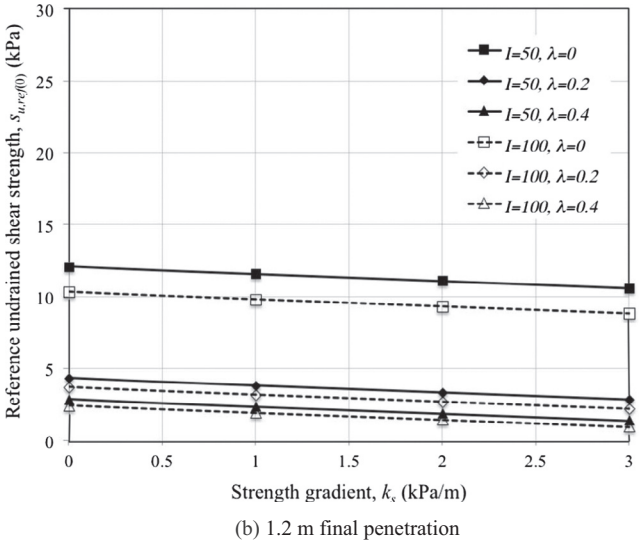

(b) 1.2 m final penetration

Fig. 13. Example interpretation of FFP test results.

Fig. 13a reveals that the value of the reference shear strength at the mudline, $s_{u,ref(0)}$, is almost independent of the strength gradient with depth, k_s. This is as expected, since in this case a FFP of diameter 0.08 m penetrates only 0.2 m into the seabed, providing limited opportunity for the gradient to have a significant effect. A small but noticeably greater effect is seen in Fig. 13b, where a device of the same dimensions penetrates much further, i.e., 1.2 m, into the seabed.

Fig. 13 also reveals the significant influence of the strength rate effect parameter, λ, on the interpreted value of $s_{u,ref(0)}$. The rigidity index of the soil, I_r, (shown in the legend simply as "*I*") also has a noticeable influence on the interpreted value of $s_{u,ref(0)}$, but this effect is not as significant as the effect of the rate parameter λ. Steiner et al. [30] also examined the effect of strain rate on dynamic penetration resistance and reported its significance. Clearly, if all that is measured in the field by a FFP is the final penetration depth, then independent assessment of the remaining strength parameters will be required to provide a definitive estimate of the undrained strength profile of the penetrated seabed.

6. Conclusions

Numerical analysis of free-falling penetrometers (FFPs) penetrating into an inhomogeneous layer of soil was considered in this study. A validated Arbitrary Lagrangian–Eulerian method was adopted to analyse these dynamic penetration problems. Numerical results indicate that the penetration characteristics of a FFP depend on the mechanical properties of the soil including its undrained shear strength, a rate parameter for strength, the rigidity index, and an inhomogeneity factor.

Closed form expressions have been suggested that closely fit the numerical predictions. These expressions relate the final penetration to the initial impact energy of the penetrometer and the strength parameters of the soil. The suggested expressions indicate that there is a quadratic relation between the final embedment depth of a FFP penetrating into an inhomogeneous layer of soil and its initial kinetic and potential energy. It was also concluded that the impact energy of a FFP is linearly related to a factor that represents the inhomogeneity of soil.

An example of the use of these proposed closed-form expressions relating the final penetration to the strength properties and rigidity index of the soil was also presented. By way of this example, it was clearly demonstrated that if all that is measured in the field FFP test is the final penetration depth, then independent assessment of the remaining strength parameters will be required to provide a definitive estimate of the strength profile of the penetrated seabed. Nevertheless, application of the closed from expressions to the measured penetration of a FFP, together with the use of typical ranges for some of the strength parameters, at least provides an indication of the possible undrained strength profile and property values for a given seabed site.

References

[1] Abu-Farsakh M, Tumay M, Voyiadjis G. Numerical parametric study of piezocone penetration test in clays. Int. J. Geomech. ASCE 2003;3(2):170–81.

[2] Aubeny CP, Shi H. Interpretation of impact penetration measurements in soft clays. J. Geotech. Geoenviron. Eng. ASCE 2006;132(6):770–7.

[3] Beard, R. M. 1985. Expendable doppler penetrometer for deep ocean sediment measurements. Strength Testing of Marine Sediments: Laboratory and In-situ Measurements, ASTM STP 883. American Society for Testing and Materials: Philadelphia, 101–124.

[4] Boukpeti N, White DJ, Randolph MF. Analytical modelling of a submarine slide under steady flow in relation to the impact load on a pipeline. Géotechnique 2012;62(2):137–46.

[5] Carter, J. P., Nazem, M., Airey, D. W. & Chow, S. W. (2010). Dynamic analysis of free-falling penetrometers in soil deposits. In GeoFlorida 2010: Advances in analysis, modelling and design, GSP 199, pp. 53–68. Reston, VA, USA: American Society of Civil Engineers.

[6] Chow SH, O'Loughlin CD, Randolph MF. A centrifuge investigation of free-fall piezocone in clay. Géotechnique 2014;64(10):817–27.

[7] Chung J, Hulbert GM. A time integration algorithm for structural dynamics with improved numerical dissipation: the generalized-α method. Journal of Applied Mechanics 1993;60:371–5.

[8] Davis EH, Booker JR. The effect of increasing strength with depth on the bearing capacity of clays. Géotechnique 1973;23(4):551–63.

[9] DeJong JT et al. Biogeochemical processes and geotechnical applications: progress, opportunities and challenges. Géotechnique 2013;63(4):287–301.

[10] Denness B, Berry A, Darwell J, Nakamura T. Dynamic seabed penetration. IEEE OCEANS 1981;13:662–7.

[11] Einav I, Randolph M. Effect of strain rate on mobilised strength and thickness of curved shear bands. Géotechnique 2006;56(7):501–4.

[12] Graham J, Crooks JHA, Bell AL. Time effects on the stress–strain behaviour of natural soft clays. Géotechnique 1983;33(3):327–40.

[13] Liyanapathirana DS. Arbitrary Lagrangian Eulerian based finite element analysis of cone penetration in soft clay. Comput. Geotech. 2009;36(5):851–60.

[14] Lu Q, Hu Y, Randolph MF. Deep penetration in soft clay with strength increasing with depth. 11th International Offshore and Polar Engineering Conference. California, USA 2001;2:453–8.

[15] Lu Q, Randolph MF, Hu Y, Bugarski IC. A numerical study of cone penetration in clay. Géotechnique 2004;54(4):257–67.

[16] Lunne, T. and Andersen, K.H. (2007). Soft clay shear strength parameters for deepwater geotechnical design. Keynote address, Proc. 6th Int. Conf. on Offshore Site Investigation and Geotechnics, London, UK, 151–176.

[17] Lysmer JR, Kuhlemeyer L. Finite dynamic model for infinite media. J. Engng Mech. Div. ASCE 1969;95(EM4):859–77.

[18] Merifield RS, Sloan SW, Yu HS. Stability of plate anchors in undrained clay. Géotechnique 2001;51(2):141–53.

[19] Nazem M, Sheng D, Carter JP, Sloan SW. Arbitrary-Lagrangian–Eulerian method for large-deformation consolidation problems in geomechanics. International Journal for Analytical and Numerical Methods in Geomechanics 2008;32:1023–50.

[20] Nazem M, Carter JP, Airey D. Arbitrary Lagrangian–Eulerian method for dynamic analysis of geotechnical problems. Comput. Geotech. 2009;36(4):549–57.

[21] Nazem M, Carter JP. Parametric study of a free-falling penetrometer in clay-like soils. In: Gourvenec, White, editors. Frontiers in Offshore Geotechnics II. London: Taylor & Francis Group; 2011.

[22] Nazem M, Carter JP, Airey DW, Chow SH. Dynamic analysis of a smooth penetrometer free-falling into uniform clay. Géotechnique 2012;62(10):893–905.

[23] Nazem M, Sheng D, Carter JP. Stress integration and mesh refinement in numerical solutions to large deformations in geomechanics. Int. J. Numer. Methods Engng 2006;65(7):1002–27.

[24] O'Loughlin CD, Richardson MD, Randolph MF, Gaudin C. Dynamic anchor embedment in clay. Géotechnique 2013;63(11):909–19.

[25] Raymond GP. The bearing capacity of large footings and embankments on clay. Géotechnique 1967;17:1–10.

[26] Scott RF. In-place ocean soil strength by accelerometer, Proc ASCE. J. Soil Mechanics and Foundations 1970;96(1):419–44.

[27] Sheng D, Nazem M, Carter JP. Some computational aspects for solving deep penetration problems in geomechanics. Comput. Mech. 2009;44(4):549–61.

[28] Skempton AW. A study of the geotechnical properties of some post-glacial clays. Géotechnique 1948;1:7–22.

[29] Stark N, Wilkens R, Ernstsen VB, Lambers-Huesmann M, Stegmann S, Kopf A. Geotechnical properties of sandy seafloors and consequences for dynamic penetrometer interpretations: quartz sand versus carbonate sand. Geotech Geol Eng 2012;30:1–14.

[30] Steiner A, Kopf AJ, L'Heureux JS, Kreiter S, Stegmann S, Haflidason H, et al. In situ dynamic piezocone penetrometer tests in natural clayey soils – a reappraisal of strain rate corrections. Can. Geotech. J. 2014;51(3):272–88.

[31] Stoll RD, Sun YF, Bitte I. Measuring sea bed properties using static and dynamic penetrometers. Civil Engineering in the Oceans 2004;VI:386–95.

[32] Stoll D, Yue-Feng S, Bitte I. Seafloor properties from penetrometer tests. IEEE Journal of Oceanic Engineering 2007;32(1):57–63.

[33] Teh CI, Houlsby GT. An analytical study of the cone penetration test in clay. Géotechnique 1991;4(1):17–34.

[34] Walker J, Yu HS. Analysis of the cone penetration test in layered clay. Géotechnique 2010;60(12):939–48.

[35] Wang D, Bienen B, Nazem M, Tian Y, Zheng J, Pucker T, et al. Large deformation finite element analyses in geotechnical engineering. Submitted to International Journal for Numerical and Analytical Methods in Geomechanics 2014.

[36] Yu HS, Herrmann LR, Boulanger RW. Analysis of steady cone penetration in clay. J. Geotech. Geoenviron. Engng ASCE 2000;126(7):594–605.